Diagn Interv Radiol DOI 10.5152/dir.2016.15331



CHEST IMAGING

ORIGINAL ARTICLE

# Pulmonary fibrosis: tissue characterization using late-enhanced MRI compared with unenhanced anatomic high-resolution CT

Lisa P. Lavelle
Darragh Brady
Sinead McEvoy
David Murphy
Brian Gibney
Annika Gallagher
Marcus Butler
Fionnula Shortt
Marie McMullen
Aurelie Fabre
David A. Lynch
Michael P. Keane
Jonathan D. Dodd

**PURPOSE**
We aimed to prospectively evaluate anatomic chest computed tomography (CT) with tissue characterization late gadolinium-enhanced magnetic resonance imaging (MRI) in the evaluation of pulmonary fibrosis (PF).

**METHODS**
Twenty patients with idiopathic pulmonary fibrosis (IPF) and twelve control patients underwent late-enhanced MRI and high-resolution CT. Tissue characterization of PF was depicted using a segmented inversion-recovery turbo low-angle shot MRI sequence. Pulmonary arterial blood pool nulling was achieved by nulling main pulmonary artery signal. Images were read in random order by a blinded reader for presence and extent of overall PF (reticulation and honeycombing) at five anatomic levels. Overall extent of IPF was estimated to the nearest 5% as well as an evaluation of the ratios of IPF made up of reticulation and honeycombing. Overall grade of severity was dependent on the extent of reticulation and honeycombing.

**RESULTS**
No control patient exhibited contrast enhancement on lung late-enhanced MRI. All IPF patients were identified with late-enhanced MRI. Mean signal intensity of the late-enhanced fibrotic lung was 31.8±10.6 vs. 10.5±1.6 for normal lung regions, $P < 0.001$, resulting in a percent elevation in signal intensity from PF of 204.8%±90.6 compared with the signal intensity of normal lung. The mean contrast-to-noise ratio was 22.8±10.7. Late-enhanced MRI correlated significantly with chest CT for the extent of PF (R=0.78, $P = 0.001$) but not for reticulation, honeycombing, or coarseness of reticulation or honeycombing.

**CONCLUSION**
Tissue characterization of IPF is possible using inversion recovery sequence thoracic MRI.

The detection and quantification of pulmonary fibrosis is important for prognosis and treatment in patients with idiopathic pulmonary fibrosis (IPF) (1, 2). The diagnosis is typically made from a combination of clinical, spirometric, and imaging criteria. High-resolution computed tomography (HRCT) is the most widely used test for image characterization. Its high spatial resolution, rapid scan times, and multiplanar capabilities make it highly suitable for detecting and characterizing pulmonary fibrosis in patients suspected of IPF (3, 4).

Other tests including magnetic resonance imaging (MRI) have been applied to the diagnosis and characterization of pulmonary fibrosis, principally in case series and cohort studies (5–8). It has several benefits in comparison with HRCT including the absence of ionizing radiation and ability to provide characterization of different tissues. Many sequences have been developed in efforts to evaluate patients with suspected IPF, and interest continues in developing sequences that may allow the detection and characterization of pulmonary fibrosis. Disadvantages include longer scan times compared with HRCT and cost, precluding its routine use in the workup of suspected pulmonary fibrosis (9).

Myocardial fibrosis detection using MRI has undergone major strides in the last two decades, such that its presence can be detected highly accurately with MRI using specific late contrast enhanced sequences (10–12). A specific double-inversion recovery sequence acquired approximately 8–12 min following intravenous contrast administration allows the detection of contrast agent that has concentrated within pulmonary fibrosis and washed out of normal cardiac tissue (13). The contrast agent concentrates in fibrotic tissue because

From the Departments of Radiology (J.D.D. ✉ *J.Dodd@st-vincents.ie*, L.L., D.B., S.M.., D.M., B.G., A.G.), Respiratory Medicine (M.B., M.P.K.) and Pathology (A.F.), St Vincent's University Hospital, University College Dublin School of Medicine, Dublin, Ireland; the Department of Radiology (F.S., M.M.), St Vincent's Private Hospital, Dublin, Ireland; the Department of Radiology (D.A.L), National Jewish Health, Denver, USA.

Received 7 August 2015, revision requested 28 March 2016, revision received 7 May 2016; accepted 4 June 2016.

Published online 9 January 2017
DOI 10.5152/dir.2016.15331

it has a larger extracellular space than normal nonfibrotic tissue, as gadolinium is an extracellular contrast agent (14). This principle has been used to detect and characterize many different types of ischemic and nonischemic cardiomyopathies (15).

We hypothesized that since late-enhanced MRI allows the detection of myocardial fibrosis, it might also be capable of detecting pulmonary fibrosis using the same principle. The purpose of this feasibility study was to evaluate whether contrast-enhanced late acquisition MRI has the ability to detect and characterize pulmonary fibrosis compared with HRCT.

## Methods

We prospectively recruited 20 patients (mean age, 67.3±9.4 years; age range, 40–79 years; 7 female and 13 male patients) with documented clinical and radiologic features of definite IPF that fulfilled American Thoracic Society (ATS)/European Respiratory Society (ERS) criteria and discussion at Interstitial Lung Disease Conference for IPF (2). Patients underwent spirometry, HRCT and a late-enhanced MRI of the thorax. Patients were excluded if they had an acute chest infection or acute exacerbation of their fibrotic lung disease at the time of their investigations. Patients with a contraindication to MRI were also excluded. Twelve randomly chosen control subjects with no cardiac or lung disease who had undergone HRCT were recruited to the study (mean age, 53.4±13.9 years; range, 35–77 years; 6 female and 6 male subjects). The local hospital ethics board approved the study and written informed consent was obtained from all subjects.

### High-resolution CT protocol

The unenhanced HRCT scans were acquired on a Siemens Sensation 64-slice CT (Siemens Healthcare) from the apices to the costophrenic angles at full inspiration at 120 kVP and 130 mAs. Contiguous slices were reconstructed at 1 mm slice thickness with a 0.5 mm increment using an edge-enhancing kernal and a 512×512 matrix. Automatic tube current modulation was utilized for all patients. Images were reconstructed using lung windows (window width 1500 HU, center -700 HU).

**Main points**

- Late gadolinium-enhanced MRI can identify pulmonary fibrosis using the histopathologic characteristics of the underlying fibrosis.
- Late-enhanced MRI is technically feasible and safe in patients with idiopathic pulmonary fibrosis.
- Late-enhanced MRI is normal in subjects with no pulmonary fibrosis.

### Thorax MRI protocol

MRI acquisition was performed on a 1.5 T magnet (GE Healthcare) with an eight-element phased-array cardiac coil (GE Healthcare) and peak gradient and slew rate. After a localizing set of axial two-dimensional (2D) steady-state-free-precession images were acquired, a bolus injection of 0.2 mmol/kg of gadoterate meglumine (Dotarem, Gd-DOTA, Guerbet) was given, followed 10–12 min later by a set of axial three-dimensional (3D) electrocardiogram (ECG)-gated double inversion-recovery prepared fast-gradient echo pulse sequences (13). Slab thickness measured 2 cm craniocaudally. Approximately 4–6 slabs were required to image the entire volume of the lungs. Each image slab required a 10–15 s breath-hold. The volume of voxels was 1.25×1.25×1.25 mm, TR/TE was 5.5/2.3 ms, inversion time was 230–310 ms, parallel imaging was applied with a speed up factor of 2, and 50 reference lines were acquired. In order to null the signal from contrast within the pulmonary circulation, inversion times were chosen based on the inversion time to null the blood pool in the pulmonary artery. For patients unable to adequately breath-hold, we used nasal prongs oxygen delivery, patient hyperventilation and a reduction in phase encoding steps to reduce sequence acquisition time.

### Image interpretation

Images were read in random order by two blinded radiologists in consensus. MRI images were read independent of the CT images. The MRI scoring system for pulmonary fibrosis was adapted from the scoring system by Desai et al. (16). Briefly, images were reviewed at five levels: 1) origin of the great vessels; 2) carina; 3) pulmonary venous confluence; 4) between levels 3 and 5; 5) 1 cm above the right hemidiaphragm. The interstitial lung disease extent was estimated to the nearest 5%. Fibrosis was divided into reticulation alone or reticulation with honeycombing. Definitions for chest CT abnormalities were based on the Fleischner society (17). Reticulation was scored as fine (1.5 mm) or thick (>1.5 mm). Honeycombing was scored as either microcystic (≤4 mm) or macrocystic (>4 mm). A predominant overall fibrosis pattern score was also given depending on: grade 1, predominant reticular pattern; grade 2, mixed pattern of reticulation and honeycombing pattern; and grade 3, predominantly honeycombing pattern. The scores from each level were averaged to give an overall extent of fibrosis score for each patient. The overall coarseness score for each patient was derived by summing the scores at five levels (minimum score, 0; maximum score, 15). In patients that had no fibrosis evident on certain image slabs, the overall score was proportionately adjusted to reflect this. Each image slab was given a confidence score for presence/absence of fibrosis using a 5-point scale (1, no confidence; 5, highly confident). For each patient individual image slab scores were summed to give a potential maximum score of 25. The same scoring system was taken for evaluating HRCT images.

### Late-enhanced MRI analysis

Regions of interest (ROIs) were placed in areas with high signal in the lungs, with a mean of three readings being taken as the average signal intensity. The ROIs were sized to avoid including adjacent normal appearing lung. The signal intensity of normal appearing lung was also recorded using similar sized circular ROIs in areas of lung showing no evidence of elevated signal. The standard deviation of image noise measured in a circular ROI outside the body was also recorded. The percent elevation in signal intensity was calculated as: 100 × (mean signal intensity of high signal intensity lung region - mean signal intensity of normal lung region)/(mean signal intensity of normal lung region) (12). Image contrast-to-noise ratios were calculated as: (mean signal intensity of the lung region of elevated signal intensity - mean signal intensity of the remote region)/1.5 × (standard deviation of noise).

### Spirometry and dyspnea testing

Pulmonary function testing was obtained using a spirometer (Pneumocheck, Welch Allyn). Forced expiratory volume in one second ($FEV_1$) and forced vital capacity (FVC) and $FEV_1$/FVC measurements conformed to current ATS/ERS standards (19). Predicted normal values were used to calculate percent predicted values for $FEV_1$ and FVC. Dyspnea was scored using the Medical Research Dyspnea scale score (range, 1.0–5.0) at the time of the MRI scan.

**Table 1.** Clinical characteristics of the study population

| Demographics | Controls (n=12) | IPF (n=20) |
|---|---|---|
| Age (years) | 53.4±13.9 | 69.2±9.6* |
| Gender (F/M), n/n | 6/6 | 7/13 |
| BMI (kg/m$^2$) | 28.3±6.3 | 27.9±7.9 |
| Spirometry (patients) | | |
| $FEV_1$, absolute | - | 2.0±0.5 |
| $FEV_1$, % predicted | - | 69.2±12.2 |
| FVC, absolute | - | 2.5±0.7 |
| FVC, % predicted | - | 61.7±17.9 |
| $FEV_1$/FVC, absolute | - | 81.3±8.2 |
| $FEV_1$/FVC, % predicted | - | 106.5±10.5 |

Data are presented as mean±standard deviation.
IPF, idiopathic pulmonary fibrosis; F, female; M, male; BMI, body mass index; $FEV_1$, forced expiratory volume in one second; FVC, forced vital capacity.
*$P < 0.01$.

**Table 2.** Differences in signal intensity between IPF and controls

| MRI signal characteristics | Controls | IPF | *P* |
|---|---|---|---|
| SI outside the body | 10.5±0.6 | 11.8±1.6 | NS |
| SI normal appearing lung | 8.5±1.5 | 10.5±1.6 | <0.01 |
| SI late-enhanced fibrotic lung | 0.0 | 31.8±10.6 | - |
| %∧F/n | - | 204.8±90.6 | - |
| Contrast-to-noise ratio | - | 22.8±10.7 | - |

Data are presented as mean±standard deviation unless otherwise noted.
MRI, magnetic resonance imaging; IPF-idiopathic pulmonary fibrosis; SI, signal intensity; NS, not significant; %∧F/n, percent elevation in MRI signal intensity of lung fibrosis compared with signal intensity of normal lung.

**Table 3.** Correlations between late-enhanced MRI and HRCT for pulmonary fibrosis evaluation

| | Controls (n=10) | | Patients (n=20) | | |
|---|---|---|---|---|---|
| Fibrosis characteristics | HRCT | LE-MRI | HRCT | LE-MRI | r |
| Presence of fibrosis, n | 0 | 0 | 20 | 20 | |
| Overall lung fibrosis extent | - | - | 42.0±15.7 | 42.1±16.0 | 0.78* |
| Reticulation % of fibrotic lung | - | - | 25.8±12.5 | 28.1±11.8 | 0.30 |
| Honeycombing % of fibrotic lung | - | - | 74.1±12.5 | 70.7±16.7 | 0.21 |

Data are presented as mean±standard deviation unless otherwise noted.
HRCT, high-resolution computed tomography; LE-MRI, late-enhanced magnetic resonance imaging.
*$P < 0.001$.

### Statistical analysis

Results are given as the mean±standard deviation with a minimum and maximum range. Univariate correlations between late-enhanced MRI fibrosis scores, HRCT fibrosis scores and spirometry were performed using Spearman rank correlation. The independent t-test was used for comparisons between IPF patients and controls. All analyses were carried out using SPSS statistical software (version 13, SPSS Inc.). A $P < 0.05$ was considered significant for all calculations.

## Results

Body mass index and gender showed no significant difference between patients and controls ($P = 0.76$), but patients in the pulmonary fibrosis group were significantly older (69.2±9.2 years vs. 53.4±13.4 years, $P = 0.01$)(Table 1). Mean disease duration from the time of diagnosis was 44±36 months (range, 3–123 months). No patients were current smokers and 12 were ex-smokers with a mean pack year history of 22. The Medical Research Dyspnea scale score was 3.0±1.5. Mean $FEV_1$ (2.0±0.5 L; range, 1.2–2.7 L) and FVC (2.5±0.7 L; range, 1.5–3.9 L) indicated a cohort of patients with moderate to severe lung impairment (Table 1).

The extent of pulmonary fibrosis was 42% (range, 14%–68%). The majority of reticulation scores in all lobes were consistent with fine rather than coarse reticulation. Honeycombing was typically microcystic. Mean percent reticulation was 33%. The confidence score was 4.8±0.3 (range, 4–5). No control patient had lung fibrosis.

Mean MRI scan time was 32.8±4.2 min (range, 25–40 min). The average heart rate during MRI scan acquisition was 75.7±11.3 beats per minute. All patients with pulmonary fibrosis and all controls were correctly identified on late-enhanced MRI (Table 2, Fig. 1). Late-enhanced MRI signal was significantly higher for pulmonary fibrosis patients compared with controls (10.5±1.6 vs. 8.5±1.5, $P = 0.01$). Late-enhanced fibrotic lung showed a mean signal intensity of 31.8±10.6 (Figs. 2–4). Late-enhanced MRI signal intensity of pulmonary fibrosis was 204.8%±90.6% increased compared with the signal intensity of normal lung. The mean MRI contrast-to-noise ratio was 22.8±10.7.

The extent of pulmonary fibrosis on late-enhanced MRI correlated significantly with HRCT (r=0.78, $P < 0.001$) (Table 3). Percentage of reticulation or honeycombing showed no significant correlations between the two modalities ($P = 0.34$ and $P = 0.23$, respectively). There was no significant correlation between late-enhanced MRI and HCRT for the coarseness of fibrosis or for the subtype of honeycombing ($P = 0.45$ and $P = 0.23$, respectively). Confidence scores between controls and patients showed no significant difference on late-enhanced MRI (22.1±2.9 vs. 23.1±2.4, $P = 0.44$). There were significant differences in confidence scores comparing late-enhanced MRI to HRCT (22.2±2.8 vs. 24.3±1.3, $P < 0.001$).

## Discussion

In this proof-of-concept study, we showed that pulmonary fibrosis can be depicted with late-enhanced MRI using a specific segmented turboFLASH pulse sequence. The key aspect of the sequence allowing application to lung fibrosis imaging is the nulling of the pulmonary arterial blood signal using an inversion time set to null the blood signal. Similar to myocardial fibrosis depiction, the increased extracellular space in the fibrot-

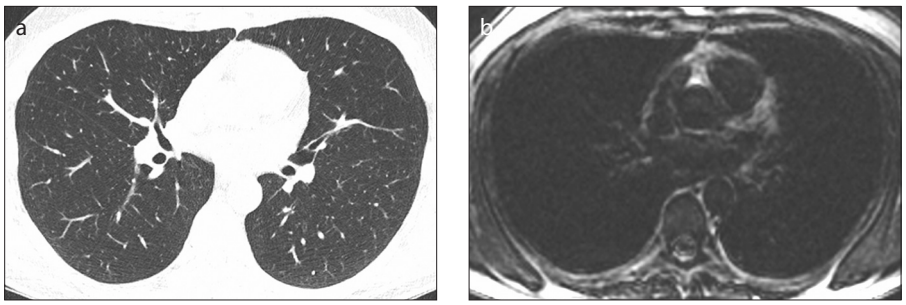

**Figure 1. a, b.** A 53-year-old control subject. High-resolution computed tomography (HRCT) image **(a)** shows normal lungs with no areas of high signal. Late-enhanced magnetic resonance imaging (MRI) **(b)** shows homogenous low signal throughout the lungs with no contrast-enhancement.

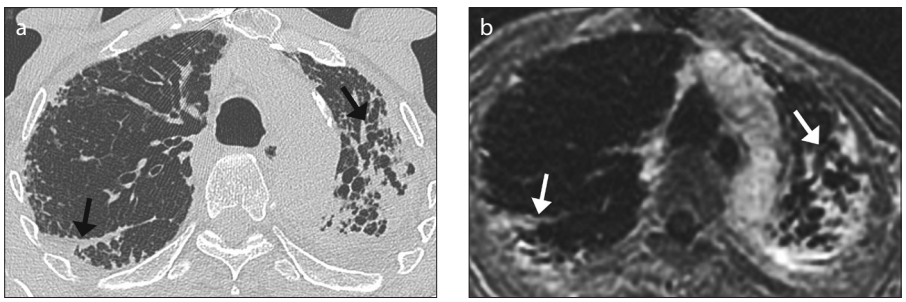

**Figure 2. a, b.** A 75-year-man with moderate idiopathic pulmonary fibrosis (IPF). HRCT image **(a)** demonstrates asymmetric extensive subpleural fibrosis *(arrows)* in the upper lobes, worse in the left upper lobe. Late-enhanced MRI of the thorax **(b)** shows extensive areas of late-enhancement *(arrows)* corresponding to the areas of fibrosis on HRCT. Note the ability to depict honeycombing and traction bronchiectasis in both upper lobes.

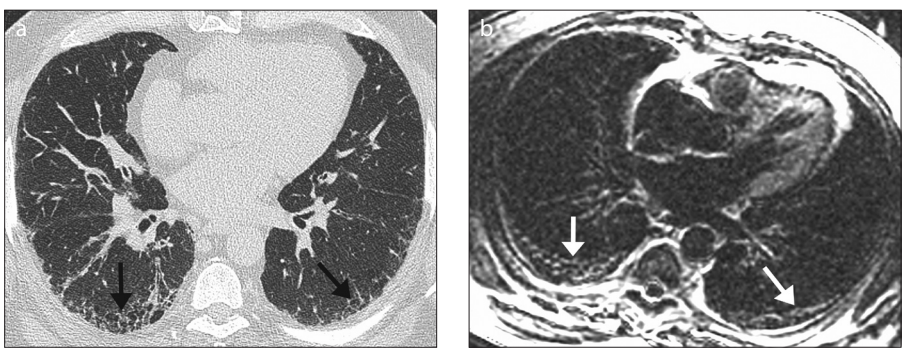

**Figure 3. a, b.** A 58-year-old man with mild IPF. HRCT image **(a)** shows symmetric mild subpleural fibrosis *(arrows)* in the lower lobes, with microcystic honeycombing. Late-enhanced MRI of the thorax **(b)** shows areas of late-enhancement and subpleural microcystic honeycombing *(arrows)* corresponding to the appearances on HRCT.

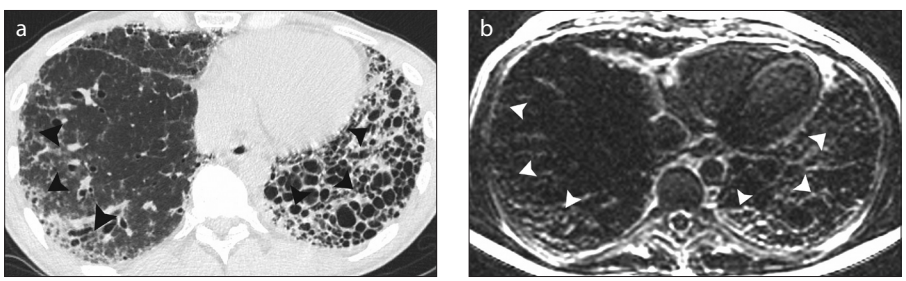

**Figure 4. a, b.** A 40-year-old man with moderate IPF. HRCT image **(a)** shows extensive macrocystic honeycombing throughout the left lower lobe *(arrowheads)*. Less severe fibrotic changes are noted in the right lower lobe *(arrowheads)*. Late-enhanced MRI of the thorax **(b)** shows corresponding extensive late-enhancement *(arrowheads)* throughout the lower lobes in keeping with diffuse fibrosis. Honeycombing is noted in the left lower lobe.

ic tissue within the interstitial space of the lung allows pooling of gadolinium, which is an extracellular contrast agent. The principle of detecting gadolinium-based contrast agents in fibrotic myocardial tissue has been extensively evaluated, and the technique is now widely applied to many different types of cardiomyopathy (10, 15). Since the fibrotic tissue in myocardium is histopathologically similar to lung fibrotic tissue, theoretically there is no reason why the cardiac MRI technique could not be applied to the detection of pulmonary fibrosis (20). There are several important differences in applying the late-enhanced MRI technique between the cardiac and respiratory systems. First, late-enhanced MRI of the myocardium relies on nulling normal myocardial tissue. When the normal myocardium is imaged at the correct inversion time or null time, it highlights fibrotic myocardium particularly well because the null time for normal myocardium differs by about 200 ms from the null time of myocardial fibrosis (21). In the lungs, the late-enhancement of pulmonary fibrosis has a similar inversion time to that of the pulmonary blood pool (the difference is 40–60 ms), and the use of a nonselective inversion recovery preparation pulse may actually suppress late-enhancement within areas of pulmonary fibrosis. Thus, the increased signal intensity from late-enhancement identified in pulmonary fibrosis is not as high as it is from myocardial fibrosis. Nonetheless, there were significant differences in the mean percent elevation in MRI signal intensity of lung fibrosis compared with the signal intensity of normal lung. The sequence does require a breath-hold of 10–17 s, which may be problematic in patients with severe pulmonary fibrosis. We used various techniques to obtain longer breath-holds such as using nasal prongs oxygen delivery, hyperventilating the patient for 15–20 s before sequence acquisition and reducing the number of phase encoding steps of the sequence, with the disadvantage of a reduction in spatial resolution. Furthermore, we used a 3D sequence to capture the lung with no slice gaps, but it is theoretically possible to only use 2D slice capture, which would result in shorter breath-holds and potentially improve image quality because they are less sensitive to motion artifact. The disadvantage is that there would be slice gaps and the requirement for many slices to adequately cover the lungs, ultimately resulting in a longer scan time and more frequent breath-holds. Despite the excellent spatial resolution of the 3D late-en-

hanced sequence, thin septal lines <1 mm in thickness were at times difficult to identify, and we were unable to accurately differentiate thin reticulation from honeycombing in some lung regions.

There is robust scientific evidence to suggest that the fibrotic tissue found in chronic myocardial infarction is of similar composition to that found in the lung. Fibroblasts are mesenchymal cells derived from the embryonic mesoderm tissue, and are not terminally differentiated. They can reactivate through several chemical signals that promote proliferation and cellular differentiation to form myofibroblasts with an upregulated rate of matrix production (22). Fibroblast activation plays a vital role in wound healing. In disease states fibroblast activity becomes deregulated in entities such as IPF and cardiac fibrosis, producing a pathologic fibrotic response. Fibroblast proliferation is particularly well validated in lung fibrosis using lineage-specific deletion of the type II transforming growth factor beta (TGF-β) receptor (23). Transforming growth factor beta (TGF-β) receptor is also widely implicated in the increased expression of fibroblasts in cardiac fibrosis (24).

Although to our knowledge we are the first to apply a double inversion ECG-gated sequence with specific pulmonary blood pool nulling for the tissue characterization of pulmonary fibrosis, others have used MRI to depict pulmonary fibrosis. One study assessing usual interstitial pneumonitis used a spin-echo sequence to depict fibrosis 5–15 min following contrast (25), but the sequence was unable to robustly depict the fibrosis because of breathing artifacts. Another study of 25 patients with interstitial lung disease demonstrated a significant difference in signal uptake at 1 and 3 min after contrast injection between inflammatory and fibrotic lesions (26). Yi et al. (27) investigated the use of dynamic contrast imaging in patients with usual interstitial pneumonia. A dynamic T1-weighted 3D multishot turbo field-echo sequence was acquired at 1, 3, 5, and 10 min in 26 patients with interstitial lung disease and found early enhancement in inflammation-predominant lesions and late-enhancement in pulmonary fibrosis. Only 41% of patients with fibrosis demonstrated late-enhancement, and the differences were not statistically different. Important additions in our approach were the use of individual inversion times to null the pulmonary blood pool and the lack of fat suppression to reduce sequence acquisition time, thus reducing breathing artifacts.

In this feasibility study, our findings have several potential clinical applications. Demonstrating late-enhancement in areas of pulmonary fibrosis may help quantify the amount of fibrosis in a given lung volume. Cardiac MRI software applications already exist that can perform this measurement for late-enhancement in areas of myocardial infarction. It would be interesting to apply this approach to the lungs using our technique. A further application is the potential ability to assist in differentiating fibrosis from mimickers such as emphysema (1, 6). We know this can be challenging even for expert readers (1, 6). This might be of particular value in patients with combined pulmonary emphysema-fibrosis syndrome, to evaluate the percentage of abnormal lung that is fibrotic (28). Such findings have implications for both clinical treatment and prognosis. Another difficulty when interpreting HRCT from an anatomical perspective relates to differentiating honeycombing from infection superimposed on emphysema, which can have similar imaging appearances. Further studies are needed to elucidate whether late-enhanced MRI of the lungs can play a useful role in these contexts.

A number of limitations of our study should be noted. First, our study was a proof-of-concept study, and further efforts are needed to optimize the sequence further for the purposes of characterizing pulmonary fibrosis. In this regard, we are currently evaluating a non-ECG gated inversion recovery sequence in order to shorten the breath-hold per slab acquisition. A related issue was the significantly younger age in our control group; although, we do not believe this substantially influenced our findings, since older patients without pulmonary fibrosis syndromes rarely show honeycombing. It was not our intention in this study to assess the optimum inversion time for depicting the pulmonary fibrosis. We applied the typically used and well validated 10-minute delay before image acquisition, which is the standard for myocardial fibrosis imaging, but in pulmonary fibrosis it may be better to wait a longer time period before imaging for pulmonary fibrosis. This would allow further wash-out of contrast from the pulmonary blood pool.

In conclusion, we describe a new technique for accurate tissue characterization of pulmonary fibrosis using late-enhanced thorax MRI with specific nulling of the pulmonary blood pool signal.

## Conflict of interest disclosure

The authors declared no conflicts of interest.

## References


1. Lynch DA, Godwin JD, Safrin S, et al. High-resolution computed tomography in idiopathic pulmonary fibrosis: diagnosis and prognosis. Am J Respir Crit Care Med 2005; 172:488–493. [CrossRef]
2. Raghu G, Collard HR, Egan JJ, et al. An official ATS/ERS/JRS/ALAT statement: idiopathic pulmonary fibrosis: evidence-based guidelines for diagnosis and management. Am J Respir Crit Care Med 2011; 183:788–824. [CrossRef]
3. Raghu G, Lynch D, Godwin JD, et al. Diagnosis of idiopathic pulmonary fibrosis with high-resolution CT in patients with little or no radiological evidence of honeycombing: secondary analysis of a randomised, controlled trial. Lancet Respir Med 2014; 2:277–284. [CrossRef]
4. Raghu G. Idiopathic pulmonary fibrosis: new evidence and an improved standard of care in 2012. Lancet 2012; 380:699–701. [CrossRef]
5. Corteville DMR, Kjørstad A, Henzler T, Zöllner FG, Schad LR. Fourier decomposition pulmonary MRI using a variable flip angle balanced steady-state free precession technique. Magn Reson Med 2015; 73:1999–2004. [CrossRef]
6. Rajaram S, Swift AJ, Capener D, et al. Lung morphology assessment with balanced steady-state free precession MR imaging compared with CT. Radiology 2012; 263:569–577. [CrossRef]
7. Ohno Y, Nishio M, Koyama H, et al. Pulmonary MR imaging with ultra-short TEs: utility for disease severity assessment of connective tissue disease patients. Eur J Radiol 2013; 82:1359–1365. [CrossRef]
8. Seki S, Koyama H, Ohno Y, et al. Diffusion-weighted MR imaging vs. multi-detector row CT: Direct comparison of capability for assessment of management needs for anterior mediastinal solitary tumors. Eur J Radiol 2014; 83:835–842. [CrossRef]
9. Ackman JB, Wu CC, Halpern EF, Abbott GF, Shepard J-AO. Nonvascular thoracic magnetic resonance imaging: the current state of training, utilization, and perceived value: survey of the society of thoracic radiology membership. J Thorac Imaging 2014; 29:252–257. [CrossRef]
10. Kim RJ, Albert TS, Wible JH, et al. Performance of delayed-enhancement magnetic resonance imaging with gadoversetamide contrast for the detection and assessment of myocardial infarction: an international, multicenter, double-blinded, randomized trial. Circulation 2008; 117:629–637. [CrossRef]
11. Kim RJ, Wu E, Rafael A, et al. The use of contrast-enhanced magnetic resonance imaging to identify reversible myocardial dysfunction. N Engl J Med 2000; 343:1445–1453. [CrossRef]
12. Kim RJ, Shah DJ, Judd RM. How we perform delayed enhancement imaging. J Cardiovasc Magn Reson 2003; 5:505–514. [CrossRef]
13. Simonetti OP, Kim RJ, Fieno DS, et al. An improved MR imaging technique for the visualization of myocardial infarction. Radiology 2001; 218:215–223. [CrossRef]
14. Kim RJ. Cardiovascular MRI. Philadelphia: WB Saunders Company; 2007.
15. O'Donnell DH, Abbara S, Chaithiraphan V, et al. Cardiac MR imaging of nonischemic cardiomyopathies: imaging protocols and spectra of appearances. Radiology 2012; 262:403–422. [CrossRef]

16. Desai SR, Veeraraghavan S, Hansell DM, et al. CT features of lung disease in patients with systemic sclerosis: comparison with idiopathic pulmonary fibrosis and nonspecific interstitial pneumonia. Radiology 2004; 232:560–567. [CrossRef]
17. Hansell DM, Bankier AA, MacMahon H, McLoud TC, Muller NL, Remy J. Fleischner Society: glossary of terms for thoracic imaging. Radiology 2008; 246:697–722. [CrossRef]
18. Smulders MW, Bekkers SCAM, Kim HW, Van Assche LMR, Parker MA, Kim RJ. Performance of CMR methods for differentiating acute from chronic MI. JACC Cardiovasc Imaging 2015; 8:669–679. [CrossRef]
19. Miller MR, Hankinson J, Brusasco V, et al. Standardisation of spirometry. Eur Respir J 2005; 26:319–338. [CrossRef]
20. Kendall RT, Feghali-Bostwick CA. Fibroblasts in fibrosis: novel roles and mediators. Front Pharmacol 2014; 5:123. [CrossRef]
21. Kim RJ, Fieno DS, Parrish TB, et al. Relationship of MRI delayed contrast enhancement to irreversible injury, infarct age, and contractile function. Circulation 1999; 100:1992–2002. [CrossRef]
22. Verrecchia F, Mauviel A. Transforming growth factor-beta and fibrosis. World J Gastroenterol 2007; 13:3056–3062.
23. Hoyles RK, Derrett-Smith EC, Khan K, et al. An essential role for resident fibroblasts in experimental lung fibrosis is defined by lineage-specific deletion of high-affinity type II transforming growth factor β receptor. Am J Respir Crit Care Med 2011; 183:249–261. [CrossRef]
24. Euler-Taimor G, Heger J. The complex pattern of SMAD signaling in the cardiovascular system. Cardiovasc Res 2006; 69:15–25. [CrossRef]
25. King MA, Bergin CJ, Ghadishah E, Yi ES, Clark JB. Detecting pulmonary abnormalities on magnetic resonance images in patients with usual interstitial pneumonitis: effect of varying window settings and gadopentetate dimeglumine. Acad Radiol 1996; 3:300–307. [CrossRef]
26. Gaeta M, Blandino A, Scribano E, et al. Chronic infiltrative lung diseases: value of gadolinium-enhanced MRI in the evaluation of disease activity--early report. Chest 2000; 117:1173–1178. [CrossRef]
27. Yi CA, Lee KS, Han J, Chung MP, Chung MJ, Shin KM. 3-T MRI for differentiating inflammation- and fibrosis-predominant lesions of usual and nonspecific interstitial pneumonia: comparison study with pathologic correlation. AJR Am J Roentgenol 2008; 190:878–885. [CrossRef]
28. Akira M, Inoue Y, Kitaichi M, Yamamoto S, Arai T, Toyokawa K. Usual interstitial pneumonia and nonspecific interstitial pneumonia with and without concurrent emphysema: thin-section CT findings. Radiology 2009; 251:271–279. [CrossRef]